UF | UNMANNED FOIL

Prototyping of a Single-Mast Electric Hydrofoil

Axton Isaly, Sebastian Deleon, Antonio Diaz, Moses Divaker, Ryan Earl, Lucas Murphy, Andrew Ortega

Faculty Advisor: Peter Ifju

Authors:
axtonisaly1013@ufl.edu
ssjdeleon@gmail.com
tony52892@ufl.edu
nyflyer@ufl.edu
rearl@ufl.edu
ldmgator@gmail.com
andrew.ortega@ufl.edu

Faculty Advisor: ifju@ufl.edu

University of Florida
Unmanned Aircraft Systems
Research Program
P.O. Box 110450
Gainesville Florida 32611
352.294.2829
uas.ifas.ufl.edu

ABSTRACT

A unique, single-mast, electric, unmanned hydrofoil vessel was developed at the University of Florida for survey and mapping (bathymetry) applications. A group of students familiar with designing and building unmanned aircraft systems were intrigued with the recent development of hydrofoil surfboards, such as the Lift eFoil. By combining the concept of the single-mast design with modern drone autopilot technology, a unique vessel was developed that has advantages over traditional small unmanned watercraft. The vessel is 72 inches long, 26 inches wide, and 42 inches tall with a total weight of approximately 120 lb, making transport, launching, and operation convenient. The advantages of this platform over a conventional watercraft are the reduced drag associated with a hydrofoil and a more stable platform that allows a sensor (such as a camera or sonar transducer) to traverse just under the water surface, at high speeds, unaffected by wind and chop. Because of the efficiencies that the hydrofoil allows the vessel has a longer range and operates for a longer duration for a given battery capacity or runs at higher speeds for a given motor/battery power. The vessel also was designed with a telescoping mast, thus allowing it to be launched in as little as 10 inches of water. This paper describes the design process that was implemented, fabrication, testing, and validation in a real-world setting. The vessel has the potential to perform a prescribed raster pattern to produce unmanned underwater surveys with sonar or optical sensors.

Axton Isaly, Sebastian Deleon, Antonio Diaz, Moses Divaker, Ryan Earl, Lucas Murphy, and Andrew Ortega

UF: Unmanned Foil
Prototyping of a Single-Mast Electric Hydrofoil

I. ABSTRACT

A unique, single-mast, electric, unmanned hydrofoil vessel was developed at the University of Florida for survey and mapping (bathymetry) applications. A group of students familiar with designing and building unmanned aircraft systems were intrigued with the recent development of hydrofoil surfboards, such as the Lift eFoil. By combining the concept of the single-mast design with modern drone autopilot technology, a unique vessel was developed that has advantages over traditional small unmanned watercraft. The vessel is 72 inches long, 26 inches wide, and 42 inches tall with a total weight of approximately 120 lb, making transport, launching, and operation convenient. The advantages of this platform over a conventional watercraft are the reduced drag associated with a hydrofoil and a more stable platform that allows a sensor (such as a camera or sonar transducer) to traverse just under the water surface, at high speeds, unaffected by wind and chop. Because of the efficiencies that the hydrofoil allows, the vessel has a longer range and operates for a longer duration for a given battery capacity or runs at higher speeds for a given motor/battery power. The vessel also was designed with a telescoping mast, thus allowing it to be launched in as little as 10 inches of water. This paper describes the design process that was implemented, fabrication, testing, and validation in a real-world setting. The vessel has the potential to perform a prescribed raster pattern to produce unmanned underwater surveys with sonar or optical sensors.

List of Acronyms

CAD	Computer-Aided Design
CFD	Computational Fluid Dynamics
IMU	Inertial Measurement Unit
LiPo	Lithium Polymer
OTS	Off-the-shelf
PWM	Pulse-Width Modulation

II. INTRODUCTION

By combining technologies from the recent advances in the development of single-mast, electric hydrofoil watercraft such as the hydrofoil surfboard Lift eFoil [1], the University of Florida has developed an unmanned hydrofoil watercraft, shown in Figure 1, that can be used for a myriad of applications as a result of fly-by-wire drone autopilot technology. The resulting vessel, called the Unmanned Foil, was designed and fabricated by a group of University of Florida students in a tiered approach. The first phase was conducted by a small group of students as part of the Mechanical Engineering Capstone Design sequence. This design was then refined and tested by members of the University of Florida Unmanned Aircraft Systems Research Program[1] (UF UASRP). The team of student authors is comprised of a combination of students from the capstone design class and the UF UASRP.

Figure 1. Various views of the Unmanned Foil. A video of the vessel in operation is available at: https://www.youtube.com/watch?v=COIa1xe7tfw

The Unmanned Foil, seen in Figure 1, is 72 inches long, 26 inches wide, and 42 inches tall (with the mast extended), with a total weight of approximately 120 lb, making transport, launching, and operation convenient. The advantages of this platform over a conventional watercraft are the reduced drag associated with a hydrofoil and a more stable platform that allows a sensor (such as a camera or sonar transducer) to traverse just under the water surface unaffected by wind and chop. Because of the efficiencies that the hydrofoil allows, the Unmanned Foil has a longer range and operates for a longer duration for a given battery

[1] Find the UASRP online at: https://uas.ifas.ufl.edu/

capacity or runs at higher speeds for a given motor/battery power.

The underwater portion of the vessel (hydrofoil) is similar to a fixed-wing airplane and is comprised of a fuselage, wing, and vertical and horizontal stabilizers. As shown in Figure 2, control of the vessel is accomplished with underwater elevons (two control surfaces on the outboard portion of the horizontal stabilizers that mimic a combination of an elevator and ailerons) that affect the pitch and roll. The wing provides lift and the horizontal stabilizer and elevons actively trim the vessel so that it remains level. A vertical airfoil-shaped mast connects the hydrofoil to the hull of the vessel. In operation, the vessel acts as an inverted pendulum (similar to a Segway®) with 75% of its weight in the mast and hull. Without the fly-by-wire functionality of the autopilot, the vessel would be unstable.

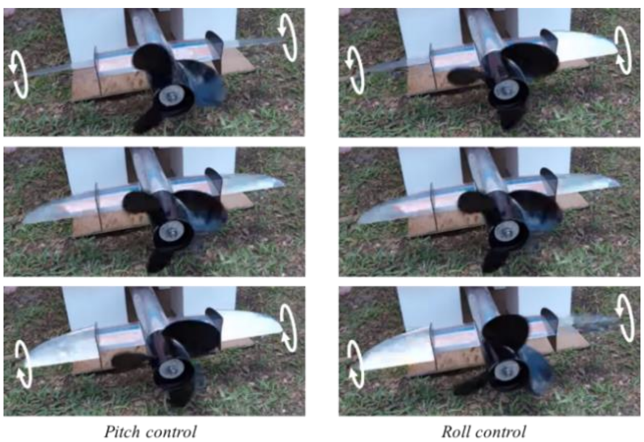

Figure 2. Pitch is controlled by coordinated rotation of the outboard portion of the horizontal stabilizer (elevons) while roll is controlled by alternate actuation of the elevons.

The Unmanned Foil utilizes an unmanned aircraft grade Pixhawk® autopilot, equipped with an IMU comprised of a 3-axis gyro, accelerometer, and magnetometer. Pressure sensors mounted in the fuselage of the vessel provide depth and velocity feedback to the Pixhawk. Measurements from the pressure sensors are used in a custom control algorithm which lets the autopilot maintain the vessel at a set elevation and speed. The vessel is also equipped with a GPS unit so that it can accurately follow navigation paths for linear or area coverage. The GPS data can be synchronized with underwater images and sonar data to map the sea-floor depth and create high-resolution digital elevation models or traditional photo mosaics.

One of the important design elements of our concept is the mast extension/retraction mechanism that allows the vessel to operate in a wide range of water depths. As shown in Figure 3, when the mast retracts, the vessel's draft is only 11 inches. It can, therefore, be launched in shallow water and controlled as a traditional watercraft out to deeper water. Once the vessel reaches depths of 3 feet, the mast extends, and the vessel can operate in hydrofoil mode, reaching speeds of up to 30 mph. The hydrofoil starts to "fly" at speeds of 8 mph with a high-speed wing, or 5 mph with an alternate larger wing. The overall speed range of the hydrofoil is 8 to 30 mph with the high-speed setup and 4 to 20 mph with the low-speed setup. Crucial to the efficiency of these two setups is the propeller selection. A custom propeller had to be fabricated for the high-speed setup since there were no commercial propellers available to match the specifications of this configuration. The low speed setup utilized a commercial OTS propeller.

Figure 3. The mast retraction mechanism in action.

The propulsion system of the Unmanned Foil is a 5000-watt electric motor and 6.71:1 gearbox optimized for 20 mph. The optimization incorporated the motor, gear ratio, operating voltage, electronic speed controller and propeller specifications. The motor operates at 44.4 volts on LiPo batteries in a series/parallel configuration comprised of four 23 Amp hour (A·h) 6S batteries totaling 23 lb (or about a quarter of the vessel weight). This allows the vessel to operate for nearly two hours at 20 mph. Longer operation time is possible through the addition of more batteries in a parallel configuration.

The design process of the Unmanned Foil produced two prototypes. Upon completion of each prototype, a rigorous testing procedure was begun. This process included model validation and development of autonomous features in the autopilot. This paper primarily details the second prototype, while at times using lessons learned from the first prototype to motivate design decisions. The testing procedure showed that the concept has potential to be useful in a variety of applications. Due to funding availability issues, further development of the prototype has not been able to proceed.

Details of the design are provided in the following sections. Section III provides background on Bathymetric mapping to motivate a targeted application for the vessel. Section IV details some of the methods from statics and hydrodynamics that were used in the early design stage. Section V details the design of the powertrain. Section VI outlines the manufacturing techniques used to fabricate the hull. The actuation mechanisms of the vessel are described in Section VII. Section VIII describes the electrical components and autopilot software that were used to achieve autonomy. Section IX describes the testing procedure that was used to validate theoretical models and further develop the software. Finally, Section X describes intended future work. The reader is referred to the Appendix for a labelled view of some of the components that are mentioned in the subsequent sections.

Advantages of the hydrofoil concept

- *Less wetted surface area than traditional boats*
- *Can run longer for a given battery capacity*
- *Can run faster for a given motor/battery power*
- *Rides level, even in choppy water*
- *Makes for a better, more stable camera platform*
- *GPS and communication through the hull*
- *Better for sonar mapping in shallow water since it rides level*
- *Quieter than traditional boats*

III. BATHYMETRIC MAPPING

The University of Florida's UASRP is an interdisciplinary group of students and professors developing drones and remote sensing technologies for natural resource applications. Recently, the UASRP has been focused on coastal and wetland mapping in order to determine the responses to hydrological changes. To acquire bathymetric data (or underwater mapping data), the UASRP investigated potential survey vessels. An autonomous survey vessel is desirable as traditional underwater photogrammetry methods are quite labor intensive, requiring a team of divers to capture the area manually. Typically, humans are unaware of the current, leading to nonuniform data. Most unmanned survey vessels operate at slow speeds and are not designed for the open ocean; they are affected by and must actively correct for chop and waves [2]. Some vessels are completely submerged, prohibiting transmission of most radio signals, which is a huge logistical hurdle for sending telemetry, control, and navigation signals to the vessel [3].

The Unmanned Foil features unique characteristics that make it advantageous when compared to traditional methods of bathymetric data capture. The characteristics of a submerged fuselage, stable flight, wide range of speed, and a waterproof electronics compartment allow it to host a variety of sensors. The vessel is unaffected by chop, allowing for smooth sonar data acquisition; it maintains consistent speed, allowing camera triggering to be consistent; and its constant depth provides uniform data between passes. Transmission of signals is reliable since the hull is lifted above the waterline. The hydrofoil's sealed electric propulsion system allows for data to be obtained in sensitive areas typically inaccessible by boat. These areas include protected marine environments and drinking water reservoirs where a pollution risk prohibits vessels that burn fossil fuels.

For this design iteration, we included compartments sized for an RGB camera and a multibeam sonar transducer in the fuselage of the vessel, which can be coupled with the existing Global Navigation Satellite System/Inertial Navigation System (GNSS/INS) unit and processing computer in the electronics compartment of the hull. The nosecone of the fuselage can be configured to accommodate various payloads. A camera mounted in this position will have unobstructed visibility. The onboard autopilot enables camera triggering by sending a PWM signal through an accessory channel, which allows for acquisition of photos based on a timer, or by GPS location. Simultaneously, the autopilot is capable of logging when the camera is triggered and the vessel's GPS coordinates, allowing for photos to be geo-tagged.

By combining sonar and photogrammetric data, colorized 3D scans of a region can be produced. Sonar systems are capable of recording to an onboard SD card while simultaneously transmitting real time data via the on-board telemetry link to an onshore processing computer. Combined with a processing software, the Unmanned Foil would be capable of producing real time sonar maps while data collection is in progress. This is advantageous to end-users since areas with data gaps can be addressed and recaptured in situ, thereby avoiding a costly second trip. By taking still images with a camera, it is possible to achieve high resolution photogrammetric processing in clear water for applications such as seagrass and coral reef mapping [4].

IV. HYDRODYNAMICS & STATICS

A. Equilibrium Analysis

Equilibrium analysis was conducted to understand the force and moment balance as a function of the Unmanned Foil's velocity. From the success of the Lift eFoil, it was readily apparent that unmanned vessel stability was achievable. To accomplish this, the vessel dynamics first had to be understood in order to distribute the mass of each component and size the lifting surfaces for stable flight. For the Lift eFoil, longitudinal and lateral balance is achieved by rider weight-shifting, as opposed to our vessel where the mass distribution is fixed, and balance is achieved through the combination of thrust variation and actuation of control surfaces. In the equilibrium analysis, at any given speed, the starting point is a free body diagram, as shown in Figure 4, where the waterline is assumed to be halfway up the mast.

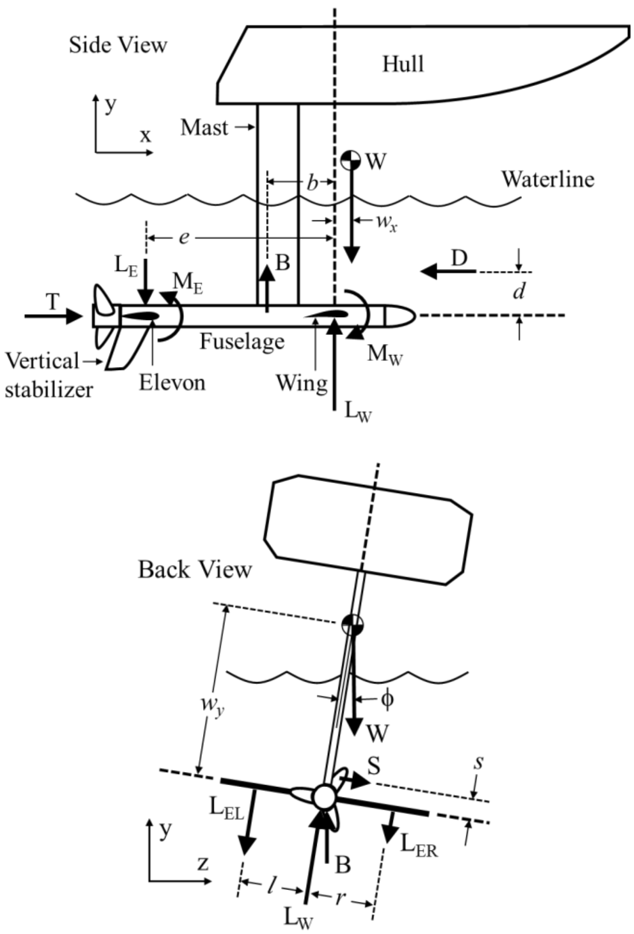

Figure 4. The free body diagrams in the x,y and y,z planes of the Unmanned Foil.

The total drag, D, is a buildup of the drag for all vessel components that are submerged and exposed to air as a function of speed. Drag analysis is presented in Section IV.B and combines the drag from the wing, D_W, elevons, D_E, fuselage, D_F, mast, D_M, vertical stabilizer, D_V, and hull, D_H. The line of action of the total drag, with respect to the center of the fuselage, *d*, is dependent on the relative drag of each component, both above and below the water. By summing forces in the horizontal direction, at any velocity, the thrust, T, must equal the total drag to maintain a constant speed, by the following equation.

$$\sum F_x = 0: T - D_W - D_E - D_F - D_M - D_V - D_H = 0 \tag{1}$$

By summing the forces in the vertical direction, shown in the following equation, we calculated the wing area and incident angle needed to carry the vessel weight, W. Unlike aircraft, the summation includes an additional term for the buoyancy, B, due to the water displaced by the submerged components. This force is centered near the middle of the fuselage. Volume calculations were made to estimate the magnitude and location of B. In the equation the wing lift, Lw, and buoyancy offset the down force on the elevons, LE, and the weight of the entire vessel (including everything above and below the waterline).

$$\sum F_Y = 0: L_W + B - L_E - W = 0 \tag{2}$$

To maintain the vessel in the upright position, moment balance calculations were made in the longitudinal and lateral directions. Moment summations were made in the x, y plane about the wing's hydrodynamic center, ca, shown in Figure 4 as a dashed vertical line, where L_w is the wing lift, and M_w is the wing pitching moment. The moment equilibrium equations are as follows, where L_E is the elevon lift (summing both sides), and M_E is the pitching moment of the elevon. Moment arms for each of the forces are shown in the figure. The longitudinal axis summation equation is presented here.

$$\sum M_{ca} = 0: D(d) + L_E(e) - L_W(w) - B(b) - M_W + M_E = 0 \tag{3}$$

The moment equilibrium in the y, z plane was used to understand the lateral balance of the vessel. In the figure the side forces (S), due to small angles of attack on the mast and vertical stabilizer are shown but are considered small and thus are not utilized in our calculations. The predominant forces that keep the vessel upright are the elevon lift on the right side, LER, and left side, LEL. This moment analysis was used to estimate the permissible tilt angle, ϕ, as a function of elevon surface area. Since most of the forces pass through the fuselage central axis, shown as a horizontal dashed line in the side view of Figure 4, they do not contribute since the moments were taken about the axis.

$$\sum M_{cf} = 0: L_{EL}(l) - L_{ER}(r) - \mathrm{W}(wy \sin \phi) - S(s) = 0 \tag{4}$$

here $r = l$ and, if we neglect side force S, this reduces to

$$(L_{EL} - L_{ER})(l) - W(wy \sin\phi) = 0 \tag{5}$$

The equilibrium equations were implemented in a spreadsheet to understand the significance of the mass of each component. To have the ability to set the location of the center of mass, the battery position was adjustable. Since batteries were expected to be on the order of 25% of the entire mass, small position adjustments of the battery had a significant effect on the longitudinal stability. The dimensions w_x and b define the static margin of the vessel. The objective was to have a positive static margin, but adjustable during field testing and gain tuning.

B. Power Polar Determination

To estimate the powertrain requirements for the Unmanned Foil, the power required to overcome the vessel's drag at a given speed must first be calculated. This power required estimation first requires an estimation of the zero lift drag coefficient (C_{D0}), also known as the parasite drag coefficient. This value was determined using the traditional component-by-component drag buildup. In the component-by-component drag buildup, the equivalent flat plate drag area is calculated, and then weighted and summed to obtain the total vessel drag. The equivalent flat plate drag area for each component (f_i) is

$$f_i = S_{wet_i} \times C_{f_i} \times FF_i \times Q_i \tag{6}$$

where i is the component index, S_{wet} is the component wetted area, C_f is the component skin friction coefficient, FF is the component form factor and Q is the component interference factor. The skin friction coefficient was obtained using the Prandtl Low Reynolds number equation [5]:

$$C_f = \frac{0.074}{Re^{1/5}} \tag{7}$$

where the Reynolds number is based on the characteristic length of each component, such as the chord, or fuselage length. The component form factors (FF) are based on the Hoerner empirical correlations [6]. These values represent the drag produced by different aerodynamic shapes:

$$Aero\ Surfaces\ \&\ Propeller\ Form\ Factor = 1 + 2\left(\frac{t}{c}\right) + 60\left(\frac{t}{c}\right)^4 \tag{8}$$

$$Fuselage\ Form\ Factor = 1 + \frac{1.5}{(l/d)^{1.5}} + \frac{7}{(l/d)^3} \tag{9}$$

In the above equations, t/c is the wing thickness-to-chord ratio (e.g 12% for a NACA0012), and l/d is the fuselage fineness ratio, where l is the fuselage length and d is the fuselage diameter. Lastly, the interference factor (Q) represents the drag produced by interaction between different components. Appropriate interference factors were obtained from Gudmunssen and are estimates based on historic data [7]. The value of 1.3 was chosen since this value is typical for un-filleted wing intersections.

Each component's equivalent flat plate area is then summed and normalized by vessel reference area and added to a miscellaneous drag coefficient term to obtain the total zero-lift drag coefficient:

$$C_{D0} = \frac{1}{S_{ref}} \sum_{i=1}^{N} f_i + C_{D_{misc}} \tag{10}$$

The miscellaneous drag term ($C_{D_{misc}}$) serves as an important "catch-all" to capture the effects of items that are hard to take into account (e.g. retraction mechanism, out-of-water boat hull, etc.) This term is hard to model a-priori, so a correction factor of 10% of the total vessel drag coefficient is used. The vessel reference area (S_{ref}) chosen was the wing planform area. N is the total number of components.

To compute the values for the skin friction coefficient, form factors and wetted areas, knowledge of the geometry of the vessel is needed. These geometry specific calculations were performed in a NASA developed parametric geometry tool known as

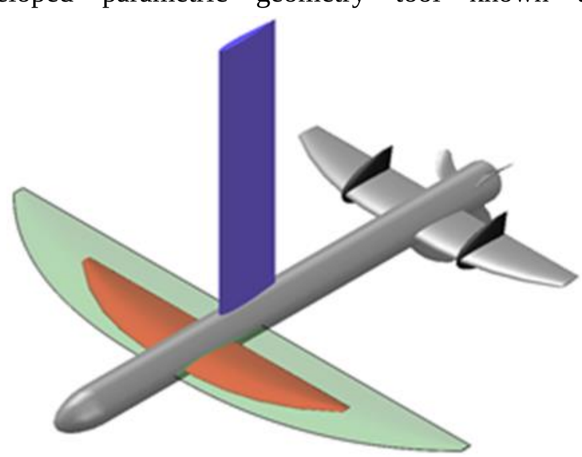

Figure 5. OpenVSP model used for drag buildup. The green wing has a planform area of 230 sq. inches, whereas the red wing has a planform area of 83 sq. inches. The vessel was mostly flown with the green wing due to better low speed handling.

OpenVSP [8]. The OpenVSP model of the vessel is shown in Figure 5.

Table I: Vessel Drag Buildup

Component	ΔC_{D0}	% of Total C_{D0}
Main Wing	0.021	37%
Stabilizer	0.008	14%
Fuselage	0.007	12%
Mast	0.010	18%
Vertical Stabilizer	0.001	2%
Wing Fences	0.002	4%
Propeller	0.002	3%
Miscellaneous	0.006	10%
Total C_{D0}	**0.0555**	100%

Lastly, the total drag acting on the vessel is based on both zero-lift drag/parasite drag and lift-induced drag. Written in coefficient form:

$$C_D = C_{D0} + \frac{{C_L}^2}{\pi ARe} \tag{11}$$

where AR is the wing aspect ratio, e is the Oswald efficiency and C_L is the operating lift coefficient. Since the objective of this effort would be to estimate the motor requirements, the power required was obtained using the drag information. The power required was obtained by calculating the force balance acting on the hydrofoil in steady wing-borne flight (i.e. lift = weight, thrust = drag) and then was multiplied by the vessel speed. This analysis was conducted for the larger wing hydrofoil shown in Figure 5 and has led to Figure 6.

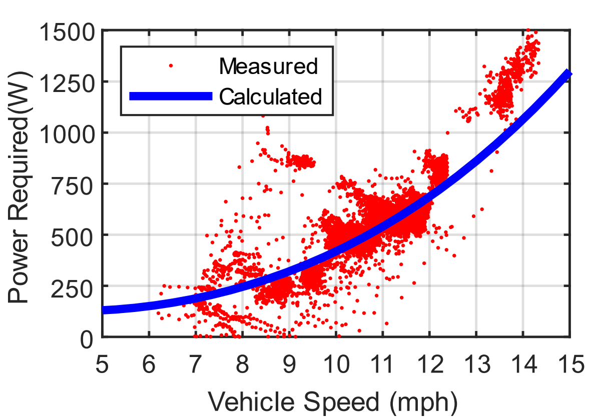

Figure 6. Hydrodynamic power required for wing-borne flight. Power data (·) measurements were converted from raw electrical power measurements to vessel hydrodynamic power assuming η_{prop} = 0.75, η_{motor} = 0.90 & $\eta_{electrical}$ = 0.95.

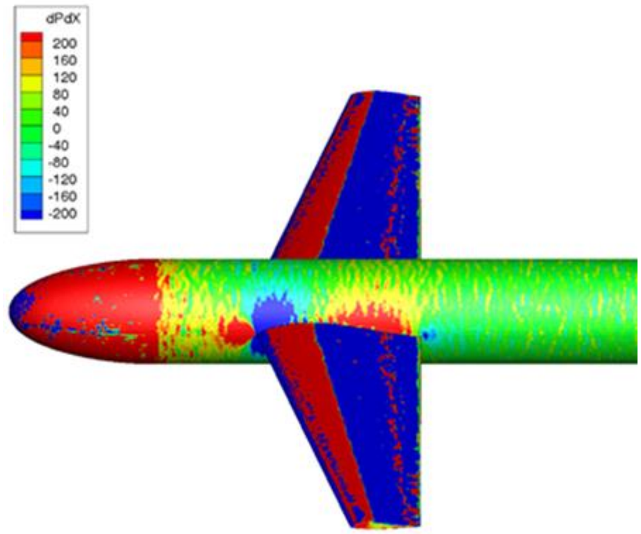

Figure 7. Streamwise pressure gradient of the front wing / fuselage combination to identify areas of small pressure gradients.

Figure 6 shows that the measured power data matches the predicted power polar very well. Power requirements substantially increase as the vessel passes through 6 mph. comparing the power required at 6 mph to 12 mph, we see that there is a 4.5x increase in the power required with a 2x increase in speed.

C. Pressure Sensor Placement

In addition to estimating the power requirements for the propulsion system, CFD simulations were also performed to estimate the location of the static port. Simulations were performed in OpenFOAM CFD software and were run on the University of Florida HiPerGator supercomputing cluster. This high-performance computer was used because of the approximately 5 million cells used in these computations. The results of the simulations are in Figure 7.

As shown in Figure 7, there is an area of a strong, favorable pressure gradient over the nose cone, and a stagnation pressure rise near the front wing. However, in-between the nose cone and front wing there is an area that has relatively small pressure gradients. This range is at least 2.14 inches ahead of the leading edge of the wing and after the nose-cone gradient. The sensor was placed 3.3 inches ahead of the leading edge of the wing and this sensor performed well and did not experience any speed related issues at this location.

V. POWERTRAIN

The Unmanned Foil's powertrain system's functional requirement was to generate, transmit, and

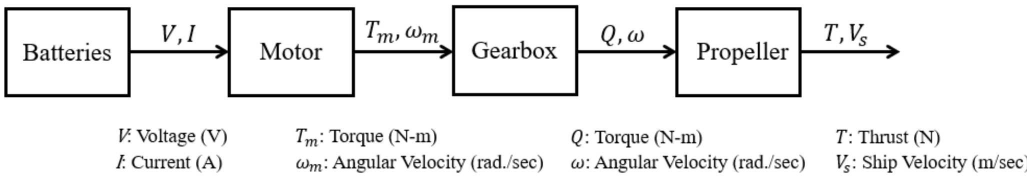

Figure 8. Powertrain component block diagram.

deliver the proper power to the water. Enough thrust had to be supplied by this system in order to overcome the maximum drag of the hull and lift the vessel out of the water, as well as provide a constant force to balance the drag of the vessel, for a fixed velocity, while on the hydrofoil. In general terms, this system included a power source (LiPo batteries), a motor (DC brushless electric motor and gearbox), transmission shafts (drive shaft, coupler, and propeller shaft), and the drive component (propeller), as summarized in Figure 8.

Although there were two different prototype versions made of this vessel, the hydrofoil's powertrain was unique when compared to the other subsystems because rather than redesign the whole system for the final iteration, the powertrain components were, instead, only modified and reused. For this reason, the initial prototype's powertrain and design constraints are presented first, with the modifications made to the final redesign given at the end. The design methodology and approach for the final Unmanned Foil version is the same as that of the first prototype, which is presented here.

Design of the powertrain subsystem first started with the selection of an appropriate commercial electric motor and propeller that could meet the desired vessel design constraints, outlined in Table II.

After selecting an appropriate OTS motor and propeller, the motor's gearbox and battery voltage/capacity would be designed and selected for optimal performance with their mating components. All component parameters (voltage, capacity, motor rpm, gear ratio, and the propeller) had to be designed *simultaneously* due to their dependence on one another. Once the first design iteration of this vessel was complete, the ultimate goal in optimizing this system involved the custom-fabrication of a propeller that would match each of the OTS motor, gearbox, and battery power supply of this craft, for a completely optimized powertrain system.

A. OTS Propeller

The first design iteration of the hydrofoil craft started with selecting a propeller to meet the vessel's maximum thrust and velocity needs. Since this vessel is unique and has a high operating velocity and low thrust requirement, the resulting propeller was selected to have a large pitch and smaller blade diameter. The following general rule of thumb for propeller selection was used, "*The same propeller can't deliver both high speed and maximum power*. A propeller sized for high speed has a small diameter and maximum pitch. A propeller sized for power or thrust has a large diameter [9]." This vessel and its propeller were designed and optimized around the high-speed craft requirements, with a small diameter and high pitch.

Table II: Powertrain Design Constrains

Design Parameter	Value
Maximum Vessel Speed, $V_{s,max}$	30 mph (13.4 m/s)
Cruising Vessel Speed, V_s	23 mph (10.28 m/s)
Cruising Time, t	2 hours
Minimum Thrust Required at Maximum Vessel Speed, T	33.72 lbf (150 N)
Propeller Hub Diameter, D	3 in (0.0762 m)
Motor Diameter, D	≤ 3 in (0.0762 m)

Table II shows the hydrofoil vessel parameters used to constrain the powertrain system.

Classical propeller design was performed with the Crouch or slip method, where the propeller's three most important factors affecting performance and efficiency—pitch, diameter, and rpm—were determined from a series of empirically derived charts and formulas based only on vessel speed and the relative slip or sliding losses between the fluid and propeller as it rotated [9]. "Cruising speed should be at 70-85% of top-rated engine RPM. Since our propeller will be of a fixed pitch, however, if it is pitched for ideal operation at 75% RPM, it will be way off at full RPM. A good average is to base pitch on operation at 90% of maximum RPM, which will yield about 90% of the maximum SHP [9]." Selection of the OTS propeller rpm and pitch is performed around 90% motor rpm (approx.) and the vessel's cruising speed (V_s). Since the cruising vessel speed was known, at a value of 23 mph (17.38 Kts), the following propeller shaft rpm (RPM) and pitch (P) were found as follows [9]:

$$P = \frac{Kts \times 1215.6}{RPM \times (1 - SlipA)} \tag{12}$$

Through a series of iterations, the propeller shaft rpm was (initially) chosen to be 1700 rpm, thus giving a prop pitch of 17.14 inches, for a slip of 27.50%. The apparent slip (SlipA) is a function of only vessel speed and was found using the following [9]

$$Slip = 1.4 \div Kts^{0.57} \tag{13}$$

It should be noted that although slip is presented here as only a function of vessel speed, the type of boat hull and its associated drag also influence the propeller's slip. For example, similar extremely fast (over 90 knots) hydroplanes have low slip values, at around 7% [9]. Were this lower propeller slip value of 7% to be used for the design (for the same propeller rpm of 1700), a pitch of only 13.36 inches would be required of the propeller.

"Diameter is the most important factor in determining the amount of power a propeller absorbs [9]." For this reason, the propeller diameter was determined around 100% of maximum RPM, and not around a lower rpm so that it did not hold down the motor rpm and vessel speed (underpropping). Diameter (D) is then calculated from maximum propeller rpm (RPM) and horsepower at the propeller (SHP) using [9]

$$D = \frac{632.7 \times SHP^{0.2}}{RPM^{0.6}} \tag{14}$$

Table III: OTS Propeller Summary

Parameter	Optimum (in)	OTS Spec (in)	OTS Prop
Pitch, P	13.36 - 17.14	15	
Diameter, D	10.15	10.125	
Hub Diameter, D_H	3	3.25	

Table III shows the OTS prop is a close match for this design.

For a 5000 W (6.71 HP) motor and max propeller speed of 1783 rpm, this yields an optimum propeller diameter of 10.15 inches. [Note: a gearbox is to be used in this design, and its efficiency is estimated at 90%, for a true SHP value of 4500 W or 6.03 HP.]

The OTS propeller chosen is summarized in Table III. The pitch is in the middle of the calculated slip range, and the blade outer diameter is a close match. The hub diameter (D_H) is similar to that of the fuselage (3 inches) for minimizing drag, and the propeller attaches with a splined shaft for easy assembly/disassembly. The prop material is aluminum and has more than the required strength for this low thrust vessel, as well as the proper corrosion resistance for this application.

B. OTS Motor and Gearbox

When selecting the motor for the hydrofoil, similar hobby-grade RC boat motor-gearbox combinations were used for comparison. Dimensionally, the motor-gearbox had to fit inside the motor pod tube, which is housed within the fuselage, and have a diameter less than 3 inches. The hydrofoil application required a high rpm, high wattage DC motor, that could have a gearbox attached to it in order to gear up the output torque necessary for the propeller, while still operating at a high rpm for optimal efficiency and low continuous current draw. A brushless motor was desired over a brushed one for better efficiency and durability. The OTS motor and gearbox selected are summarized in Table IV.

Table IV: OTS Motor-Gearbox Summary

Parameter	Value	OTS Motor-Gearbox
Model No.	Neu2230-12	
Turns	1.5Y	
KV (RPM/V)	485	
R (Ω)	0.007	
Max RPM/ Max Power (W)/ Max Voltage (V)	40,000/10,000/72	
I_0 at 10 V (A)	1.80	
Continuous Power (W)	5,000	
P62 Gearbox Ratio	6.71:1	

Table IV shows the specs for the brushless DC motor-gearbox.

From these motor parameters, the torque vs. speed/power/efficiency plots of this motor were found to determine the best operating rpm to match the propeller and maximize motor efficiency/minimize current draw. Basic electric motor relations of voltage (15), torque (16), K_T (17), K_v (18), and power (19) are given below

$$V = IR + K_e\omega \tag{15}$$

$$T = K_T I \tag{16}$$

$$K_T = \frac{60}{2\pi K_v} \tag{17}$$

$$K_v = \frac{1}{K_{e-rpm}} \tag{18}$$

$$P = T\omega \tag{19}$$

By rearranging and substituting (16) through (18) into (15), the motor overload line for a given rpm (n) as a function of only torque (T) can be found. For a voltage of 22.2 V and the motor parameters in Table IV, (15) is further simplified to the following for our motor

$$n = 10{,}767\ rpm - \left(172.43\ \frac{rpm}{N \cdot m}\right) T \tag{20}$$

Next, motor efficiency is defined in (21) using torque, speed, voltage, and total current (load and no-load). Total current is defined by (22) from the no-load current (I_0)

$$\eta_{motor} = \frac{T\omega}{VI_{total}} \tag{21}$$

$$I_{total} = I_0 + I \tag{22}$$

Using (22) in (21), the motor efficiency for a given rpm and torque value is given for the OTS motor

$$\eta_{motor} = \frac{Tn}{(381.6 + 10{,}767T)} \tag{23}$$

Plots of the motor overload, power, and efficiency as a function of torque are shown together in Figure 9, as well as the optimal operating points for rpm, torque, power, and efficiency.

The motor operating point was set to properly match the OTS propeller design rpm, as well as have the motor operate near its most efficient point, as is summarized in Table V.

Table V: OTS Motor & 6.71:1 Gearbox Summary

Parameter	Symbol	Cruising Speed, 23 mph (10.28 m/s)	Maximum Possible Value
Motor Speed	n_m	10,267 rpm	10,767 rpm
Propeller Speed	n_p	1,700 rpm	1,783 rpm
Motor Torque	T_m	2.9 N·m	62.4 N·m
Propeller Torque	Q	17.5 N·m	376.8 N·m
Motor Efficiency	η_{motor}	94.2 %	95.3 %

Table V shows the motor-gearbox values at cruising speed match the previously designed OTS propeller and are at a high motor efficiency for this hydrofoil design.

The gearbox used with this motor had a 6.71:1 ratio. This relatively high ratio was chosen to have the motor operate near its maximum efficiency point (high rpm) yet still have enough torque to spin the propeller. Gear ratio torque and rpm calculations were found from (24),

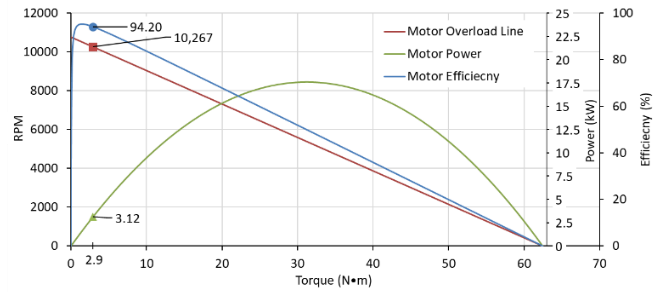

Figure 9. Optimal motor operating conditions for cruising speed.

conservatively assuming a 90% efficient gearbox, $\eta_{gearbox}$ and where ${}^{\omega_m}/_{\omega_p} = 6.71$

$$T_m\omega_m\eta_{gearbox} = Q\omega_p \tag{24}$$

C. Batteries

The selection of the power source for the hydrofoil was constrained around minimizing hull weight, while still ensuring a 2-hour runtime at the cruising speed was achieved. As a result, lightweight, LiPo electric batteries were selected over other battery or fuel alternatives.

The design of the amount of voltage and capacity for these battery packs came from the rest of the powertrain components alone—motor, gearbox, and propeller torque—operating at the cruising conditions. Determining the actual amount of torque exerted by the propeller at this vessel and shaft speed was simulated using optimized rotor design with *OpenProp* [10]. The resulting performance curves, dimensionless parameters, and propeller torque are shown in Figure 10.

At the cruising vessel speed, the OTS propeller will generate a torque Q of 12.121 N·m. This torque is not overloading the motor-gearbox capability for the specified shaft speed, as previously calculated in Table V. Furthermore, this simulation agrees with the OTS propeller design/selection, where the propeller is shown to be operating at an efficiency of 71.5 %, close to its maximum point.

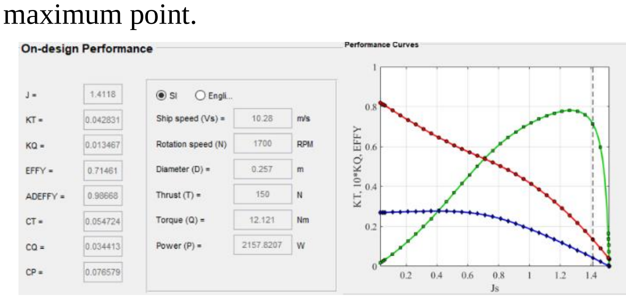

Figure 10. OTS propeller performance characteristics at cruising vessel speed.

From (24) and (16), the hydrofoil will require a continuous motor supply current of 101.9 A (powertrain only) at cruising speed. At a 2-hour runtime, this requires a battery capacity of 203.9 A·h. For this propeller torque and current, the supply voltage necessary is then calculated from (15). This is found to be 21.86 V. As a result, a 22.2 V 6S LiPo battery was selected for the hydrofoil battery, summarized in Table VI.

Table VI: Battery Summary

Parameter	Value	Battery
Model No.	LiPo 23,000 6S 22.2 V	
Voltage	22.2 V	
Capacity	23 A·h	
Type	LiPo; 6 Cells, in Series	
Discharge Rate	25C	
Weight	2478 g (5.46 lb)	

Table VI shows the specs for the LiPo batteries.

In order to achieve a 2-hour runtime, 9 of these batteries would be wired in parallel to get 207 A·h and exceed the 203.9 A·h calculated for the capacity required for the motor at cruising speed.

Table VII: Redesigned Hydrofoil Motor

Parameter		Prototype #1	Prototype #2
Motor		5000 W, 485 KV NeuMotor	5000 W, 240 KV NeuMotor
Gearbox		6.71:1 ratio	6.71:1 ratio
Voltage		22.2 V	44.4 V
Motor No-Load RPM		10,767	10,656
Motor Stall Torque		62.44 N·m	50.47 N·m
Max Prop RPM		1,783	1,590
Continuous Current Draw, I	5 mph	77.8 A	39.1 A
	10 mph	83.8 A	41.9 A
	15 mph	93.3 A	46.6 A
	20 mph	101.8 A	50.9 A
	25 mph	111.0 A	55.4 A
	30 mph	121.4 A	60.5 A

Table VII shows that the redesigned motor for prototype #2 has a current draw of half that of prototype #1 across all vessel speeds. The doubled voltage allows the same approximate motor speed to be reached.

D. Unmanned Foil (Second Prototype)

After initial testing and proof of concept, the hydrofoil prototype was redesigned to improve upon the first iteration. Namely for the powertrain, the motor current draw and propeller were completely redesigned for better longevity and improved efficiencies.

To lower the continuous current draw of the electric motor, the excitation voltage was doubled from 22.2 V to 44.4 V and the motor K_v was approximately halved from 485 to 240. Lowering the motor's K_v increases its torque constant K_T, shown in (17). Since K_T is also inversely proportional to current I (16), this will have the intended effect of halving the current draw. By doubling the voltage, the propeller shaft was able to still be spun at approximately the same speed. This design improvement is recalculated and summarized for the rewound motor in Table VII.

The Unmanned Foil was also optimized around a lower cruising speed, at 20 mph (8.94 m/s), than the first prototype. At this speed for a 2-hour runtime, the battery capacity would need to be 101.8 A·h. Five batteries wired in parallel would be required to achieve this capacity. However, since the voltage doubled, there would have to be another set of 5 batteries wired in series to this, for a total of 10 batteries for a 2-hour flight time. Due to economic constraints, the vessel opted to use 4 total batteries, resulting in the power schematic shown in Figure 11, which gives a theoretical operating time of just under 1 hour (54 mins).

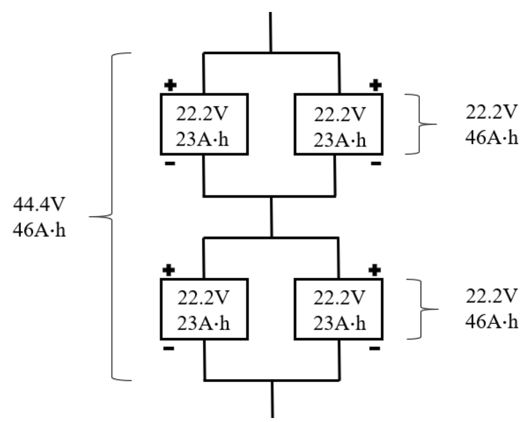

Figure 11. Prototype #2 battery schematic.

Design of the custom-fabricated propeller was performed around the revised 20 mph cruising speed and the redesigned motor-battery combination. In order to allow the propeller to be more capable of a higher vessel speed, the propeller was also designed for 75% of the Wide-Open Throttle (WOT) max prop speed or 1192 rpm. This lower shaft speed meant the prop's pitch had to be considerably steeper. Analysis was performed with *OpenProp* in order to craft a more-optimized propeller capable of higher-end speeds for this hydrofoil. Program inputs are shown in Figure 12 and its performance results are shown in Figure 13.

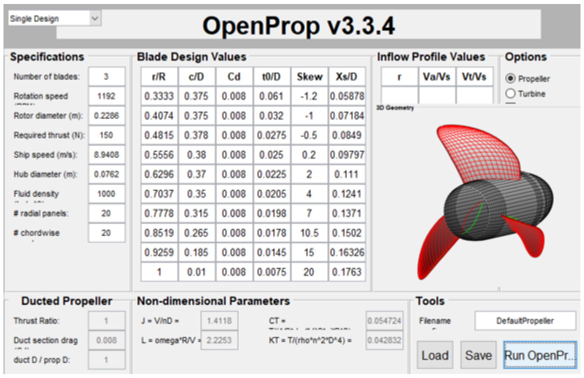

Figure 12. Custom propeller geometry and design parameters.

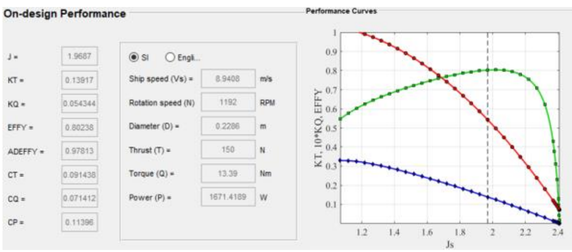

Figure 13. Custom propeller performance curves.

From the performance curves in Figure 13, the custom propeller is clearly capable of higher advance ratios (Js) than the OTS propeller and has a higher, flatter efficiency curve across these mid to high J values. This indicates a propeller designed for broader and higher range of vessel speeds, and ultimately higher efficiencies at these speeds. The custom propeller efficiency is 80.2% at the cruising speed of 20 mph.

Due to the high rpm of both prototypes' propellers, a cavitation analysis was performed in *OpenProp* [10]. The results in Figure 14 show the suction side face to have the lowest pressures, as expected, but none that caused cavitation $\left(-\frac{CP}{sigma} \geq 1\right)$.

Fabrication of the custom propeller was done on a 3-axis CNC mill, from a 9-inch OD 6061 Aluminum round stock. This was particularly challenging since the part had to be flipped and supported with jig plates to machine the underside of the blades. Pictures of the machining process and final propeller are shown in Figure 15.

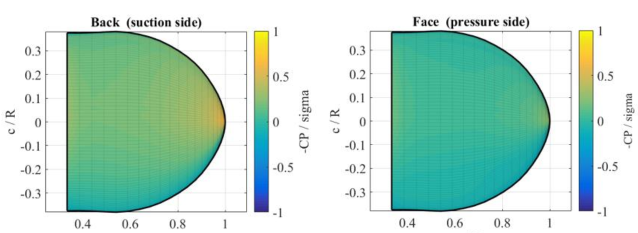

Figure 14. Cavitation analysis of custom propeller.

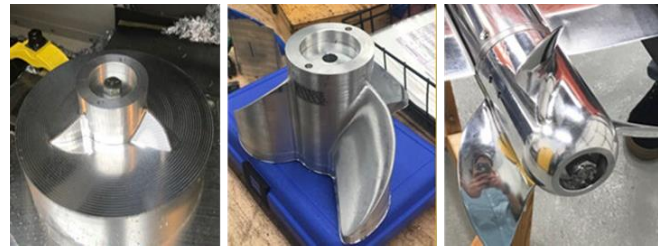
Figure 15. Images from the machining of the custom propeller.

VI. HULL DESIGN

A. Hydrodynamic Properties

An early choice in the design of the hull was whether to have a planing hull or a displacement hull. A displacement hull cuts/ploughs through the water, pushing it aside. For cruising, it generally offers better stability and efficiency than other hulls, but it is not optimal for speed and agile handling. A planing hull produces hydrodynamic lift that raises it out of the water, reducing its wetted surface as it skims atop the water surface. The planning hull is capable of higher speed, acceleration, and agility over a displacement hull, although the planning hull is less efficient and requires more power to maintain its lift [11].

The Unmanned Foil was intended to spend the majority of its time up on the foil (with the hull entirely out of the water). The only time the hull was expected to be in the water was at low speeds when either starting or stopping. Thus, the hull type was selected based on its slow speed/starting characteristics. The planing hull's hydrodynamic lift helps the craft get onto the foil faster and in a shorter distance. As the hull does not spend much of its time in the water, any cruising stability and efficiency traits that a displacement hull can offer are irrelevant. Thus, the planing hull was the clear choice for this project.

Next, specific geometric features were chosen for the hull. It was to have a shallow draft, large nose rocker, hard and pronounced 45-degree chines, a wide flat bottom, and a flat 90-degree transom. The wide and flat design would provide strong lift when accelerating from a stop and trying to get up on the foil. The overall size of the hull was chosen conservatively to provide ample room for mounting components during prototyping as well as providing sufficient buoyancy to accommodate a sizeable payload during prototyping. Figure 16 shows the CAD model of the chosen hull design.

Upon selection of a hull shape, size, and geometry, a construction method was selected. Durability and performance were the primary desired attributes. Given

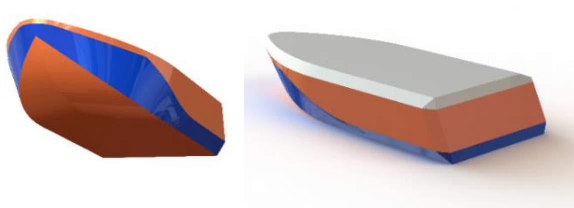

Figure 16. CAD model of hydrofoil hull, front profile and side profile.

the prototyping nature of the vessel, it was important that it be able to withstand numerous bumps, scrapes, and impacts without taking on water or incurring severe damage or downtime. This ruled out any hollow construction that could fill with water if cracked or punctured (molded fiberglass, rotomolded plastic, etc.). For a both strong and lightweight hull, a foam core fiberglass construction was chosen (similar to how surfboards and stand-up paddleboards are made). The shape of the hull would be cut with a hotwire out of a block of 1 lb/ft^3 expanded polystyrene (EPS) foam (Figure 17). Then 1/8 inch thick sheets of Divinycell foam were traced and cut out to cover all surfaces of the foam core (Figure 18). Sheets of fiberglass, Divinycell, and carbon fiber were layered onto the foam core in two curing stages: first, a layer of fiberglass covered by a layer of Divinycell foam, and, second, another layer of fiberglass, a few layers of carbon fiber on areas in need of reinforcement, and several layers of fiberglass on top of that (Figure 19). In each of the composite layup stages, the material was draped over the foam core, wetted with epoxy resin, covered with perforated release film, covered in breather material, and then sealed inside a vacuum bag for the duration of the resin cure. Upon completion of the composite layup and curing, the hull was sanded and painted.

Figure 17. Cutting EPS core with a hotwire.

To house batteries, electronics, and sensors, large cavities were cut out of the hull and turned into watertight compartments. The composite shell was cut with an oscillating multi-tool while the foam core was hollowed with a long, serrated saw and an orbital sander. A similar method was used for creating a cavity for the mast. To route wires, conduit channels were cut to connect the cavities. Watertight storage boxes intended for permanent installation on fishing boats were fitted into the cavities cut into the hull. Mounting brackets were designed and fixed within the boxes for installing electronics.

Figure 18. Divinycell foam cutouts for surfaces of the EPS hull core.

Figure 19. Laying a woven fiberglass sheet on the hull and wetting it with epoxy resin.

B. Mass and Buoyancy Distribution

The center of mass, center of buoyancy, and center of lift of the Unmanned Foil, shown in Figure 20, had to be precisely coordinated for optimal stability and performance. For optimal flight characteristics, the center of mass needed to be slightly in front of the center of lift on the wing. The center of buoyancy needed to be directly above the center of mass for the boat to sit level in the water. SolidWorks was used to create CAD models of the hull, mast, and wing assembly, and the weights of all components of the boat were recorded. All the components were assembled in SolidWorks, and the hull, mast/wing assembly, and electronics compartments were allowed to shift fore and aft with respect to each other. The centers of mass, lift, and buoyancy were dynamically simulated in the model, and components were adjusted until the points were properly aligned. The results of this design step were used to determine where on the hull to cut cavities for the mast and electronics boxes. Ergonomic handles were placed on each side of the vessel at the center of gravity for two person transport (Figure 3).

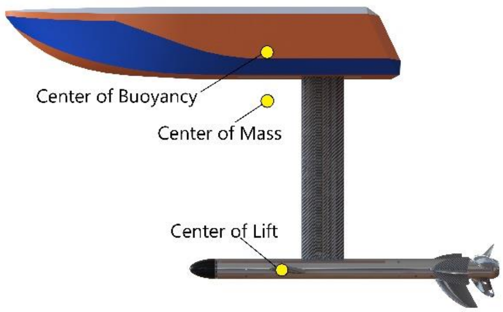

Figure 20. Center of mass, buoyancy, and lift of the Unmanned Foil.

VII. ACTUATION MECHANISMS

A. Mast and Retraction

The retraction mechanism subassembly consists primarily of a composite mast, rack and pinion, geared motor, and mast guideway (Figure 21). Shaft couplers and bearings isolate loads from the pinion to the geared motor. The retraction subassembly is housed within two compartments, where the motor is isolated in a sealed compartment, and the mast and guide system are mounted on a base plate in the rear wet area. Inductive proximity sensors act as stops to prevent the mast from being actuated past the teeth of the rack. The proximity sensor circuit will be discussed in further detail in Section VIII.A.

The retractable mast expands the mission profile of the Unmanned Foil by combining the benefits of a short mast, with its land transport and shallow-water navigation, and the benefits of a long mast, such as flying over choppy water. When the mast is retracted, the craft is made portable for convenient transport, such as in a truck bed. Manual deployment to waterfront, even in remote locations, by only two individuals is possible. The shorter length can navigate shallower waters before running aground when navigating below takeoff speed.

The initial prototype utilized an extruded aluminum OTS windsurfing hydrofoil mast from Neil Pryde. It was observed that the mast was somewhat flexible during testing. Thus, in the final version of the vessel, the mast was wrapped with 8 layers of 6-ounce carbon fiber, plain weave.

The hollow mast was leveraged to avoid external wire routing. Cavities in the mast were large enough to accommodate three 10 Ga wires for the propeller motor in addition to wires for the servo motors and pressure sensors. A custom mast-to-cable hose interface was designed so that wires could pass into the mast from the compartment containing the geared retraction motor (Figure 21). A cable hose system is used to ensure the mast and compartment are sealed from water intrusion.

Functionality of a remotely deployable mast is dependent on a mechanism that can consistently actuate and support the weight of the hull without slipping. The retraction mechanism must overcome the static weight and dynamic forces as the inertia of the hull and fuselage act on the mast beam. Bending forces acting on the mechanism are sustained by the mast guides. To accommodate for dynamic forces parallel to the face of the mast, two times the static weight of the hull assembly was chosen as the holding force and driving torque required of the DC electric motor. When the retraction motor is not running, the joint must remain rigid, and the mechanism should not consume power. For this reason, a non-back drivable motor was selected as the locking mechanism of the retractable mast. A 12-volt right-angle worm geared motor fulfills this role while meeting the required torque when coupled with a 16 tooth 1-inch diameter by 0.75-inch steel pinion gear and accompanying 32-inch rack.

The mast guide was cut and milled from aluminum plate and a plastic insert was cut to closely conform to the mast airfoil shape and create a low-friction interface for translation (Figure 21). The geared-motor mount was machined for the bolt pattern and welded. The mast-to-cable hose interface was machined in three parts on a CNC mill.

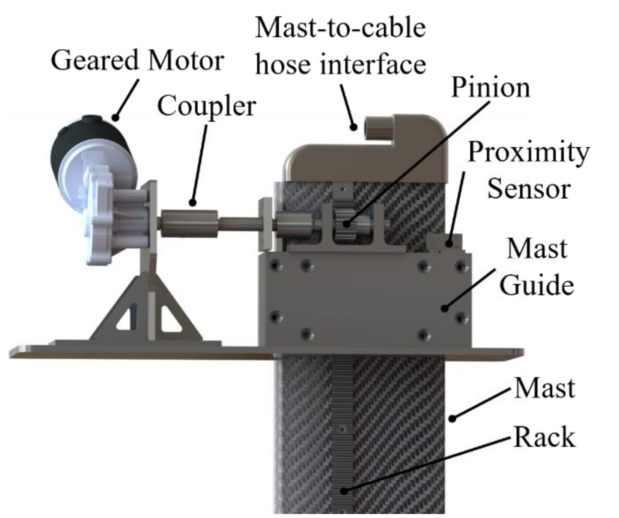

Figure 21. Telescoping mast subassembly CAD. The geared motor is housed in a separate sealed compartment.

B. Empennage

The empennage consists of aluminum outboard-mounted elevons and inboard-mounted static portions, separated by carbon fiber composite wing fences (Figure 22). Shafts, fixed to the elevons with set screws, are actuated by servo motors. Control horns are fixed to the ends of the shafts and to the servo motors. Rigid linkages with threaded rod-ends connect the horns.

The empennage design is guided by structural, functional, and environmental parameters. Structurally, the tail must withstand dynamic lift and drag loads experienced while meeting its control functionality in roll, pitch, and yaw. Starboard and portside tail-wing mounted elevons can provide all three rotations of control authority. The benefits of only two control surfaces include fewer moving parts for fabrication, assembly, and maintenance, while also reducing environmental intrusion sites. A lesson learned from the first prototype is the need for larger elevons farther from the center of gravity to impart greater control authority. The wing fences also improve control authority by maintaining the effectiveness of the elevons at high degrees of actuation, preventing spanwise propagation of flow separation. A symmetric airfoil NACA0012 was chosen for a combination of hydrodynamic performance and to accommodate the diameter of the internal shaft necessary for torsional rigidity and strength.

The maximum torque that the servo motors must support was estimated using the expected range of motion of approximately $\pm 20°$ to the flow by modeling the elevons as a flat plate. Knowing the maximum drag coefficient of the airfoil selected for the horizontal stabilizer allows this value to be doubled and serve as a conservative factor of safety for any condition the control surface experiences. The elevon shaft torque was determined by calculating the drag force on the elevon at the maximum velocity of the vessel. The shaft is located at the quarter chord of the elevon (approximate hydrodynamic center) to reduce the torque experienced. Additionally, the bending and shear of the elevon shaft were calculated and used in the selection of appropriate support bearings. The elevon is prevented from rotating about the shaft via set screw pins loaded in shear and analyzed with maximum shear stress failure criterion.

The horizontal tail was milled from aluminum and subsequently cut into the elevon and static portions (Figure 22). Grooves in the elevon shafts were turned on a lathe to accommodate O-rings for sealing. D-shaped aluminum blocks were milled to house elevon shaft bearings and allow for the horizontal tail assembly to be bolted together. The servo tray assembly was

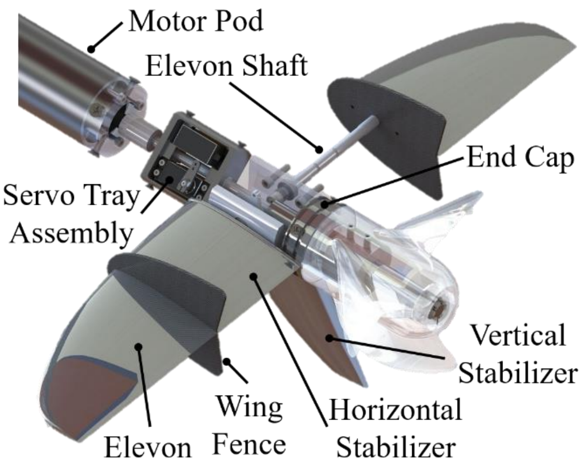

Figure 22. Tail Subassembly CAD.

milled with thru holes to allow for motor shaft access and control horns to be bolted to the cylindrical fuselage. The wing fences were cut on an abrasive waterjet from sheets of carbon fiber composite. Environmental degradation was addressed externally with corrosion-resistant material selection, including 6061-T6 aluminum for machined components.

C. Seals

A critical design aspect of the hydrofoil is that both the fuselage and hull compartments must be watertight. The fuselage must prevent water intrusion up to depths of approximately 10 feet. During the design process, the most vulnerable locations were identified as the rotating shafts of the elevons and propeller since dynamic sealing was required there. The propeller shaft is sealed with a dynamic rotary seal that was press-fit into the endcap. Furthermore, clearance was allowed behind the dynamic seal to create a grease chamber that captures any intruding water. The elevon shafts, which rotate at significantly lower speeds than the propeller shaft, are sealed with O-rings mounted in grooves cut into the shafts. These seals interface with the interior of the elevon housing, a configuration that is suggested in Section V of [12]. All other seals in the fuselage are static and fitted with O-rings in standard configurations. Notably, holes for fasteners have been countersunk and sealed with O-rings beneath the head of a flat head screw. Silicone sealant was applied in key areas (e.g., connection between the wing and fuselage) to create effective, semi-permanent seals.

The compartments of the hull are constructed using OTS boating compartments. The mast compartment is designed to be flooded, while the interface with the retraction motor shaft is fit with a dynamic seal to prevent water intrusion into the retraction motor compartment.

VIII. ELECTRONICS AND CONTROL

A. Electrical

The Unmanned Foil's electrical system was designed to allow for the distribution of power to all the hydrofoil's functional components and to allow for wireless and autonomous control of the vessel. Power from the hydrofoil's batteries had to be distributed at various voltage levels throughout the vessel. This power was used for the vessel's propeller, elevons, retraction mechanism, sensors, and communication equipment. A wiring diagram of the hydrofoil's electrical system is shown in Figure 24. The hull of the hydrofoil is divided into 3 main compartments (Figure 23). The front compartment houses telemetry, GPS, and receiver components, thus creating space between sensitive communications equipment and the high-power electronics. The middle compartment houses the hydrofoil's batteries, Pixhawk, and voltage conversion components. This placement allows the batteries to be nearest the vessel's center of gravity as they make up the bulk of its weight. The rear compartment houses components for the retraction mechanism and the connection to the mast chimney and fuselage. Wires run out of the rear compartment and into the hollow mast to the fuselage connecting to the propeller motor, the elevon servos, and the additional sensors located there.

The hydrofoil is powered by four 22.2 v 23 A·h 6S batteries (BATT). These batteries were paired together and connected in series and then in parallel to provide a 44.4 v output to the electrical system. This connection to the batteries is directly connected to the manual power switch (PS) that is used to disconnect all power

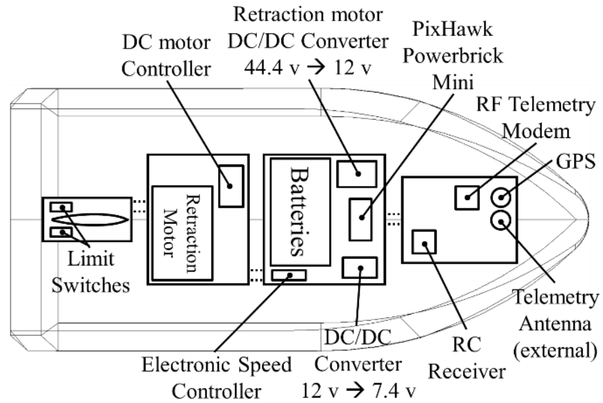

Figure 23. Compartmental layout of electrical components in the hull

to the vessel. The batteries are then connected to the propeller motor's electronic speed controller (ESC) that is used to convert the DC power from the batteries to 3-phase AC power used for the 3-winding propeller motor (PROP). The ESC can run the propeller in forward or reverse. Apart from the ESC, the batteries are directly connected to the voltage regulator (VREG), which reduced the voltage from 44.4 v to 12 v, which is used throughout the rest of the vessel. The output of the VREG is split down two paths. The first path connects to two buses that are used for the vessel's retraction mechanism (BUS), and the second path passes through the Pixhawk power supply (PPS), which converts the 12 v power to the Pixhawk's (PIX) input power of 5 v. The second path continues to the battery elimination circuit (BEC), which drops the voltage from 12 v to 7.4 v, which is then applied to the Pixhawk's servo rails.

The two buses that are wired to VREG are used as a connection point to provide power to the components

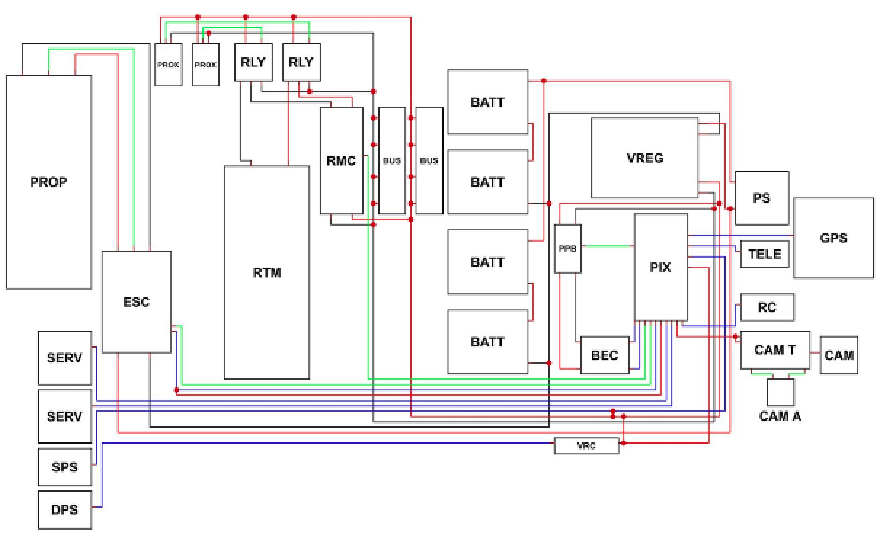

Figure 24. Hydrofoil Wiring Diagram.

that control the retraction mechanism motor (RTM). The buses connect to the retraction motor controller (RMC), which has outputs connected to two single pole double throw (SPDT) relays (RLY). These relays were controlled by the RMC and two proximity sensors (PROX) that were activated by inserts at the top and bottom of the mast of the hydrofoil. The activation of the relays controls the direction of the RTM, which then lowers or raises the mast. The relays' default state connects the terminals of the motor (which are connected to the relay's common terminals) to the RMC, which are connected to the normally closed terminals of the relays. When the RMC directs power to one relay or the other, the motor can run in forward or reverse. The proximity sensors that are connected to the coils of the relays are activated when inserts at the bottom or top of the hydrofoil's mast come into proximity with the face of the sensor. When the sensor is activated it closes a switch that allows power to flow through the coil of the relay. This switches one of the relays from its normally closed position to its open position disconnecting one of the motor terminals from the RMC and preventing the motor from running. These proximity sensors prevent the retraction mechanism from being raised or lowered outside of a desired range while still allowing the mechanism to be directed in the opposite direction from where it was stopped.

The Pixhawk 2.1 is the main hub for the hydrofoil's electrical system. It allows for control of the propeller, elevons, and retraction mechanism, and has the capability to process signals from telemetry equipment and sensors to allow for wireless manual control of the vessel as well as autonomous control through software installed on the Pixhawk. The Pixhawk has a built-in IMU comprised of a 3-axis gyro, accelerometer, and magnetometer. The IMU is used extensively with the Pixhawk's fly-by-wire functionality that automatically stabilizes the vessel when flown manually or autonomously. The Pixhawk is additionally connected to a global positioning system (GPS), a remote-control transmitter (RC), and a telemetry receiver (TELE), which are used to manually control the vessel, send and receive data, and follow predetermined paths autonomously. The servo rails allow for the Pixhawk to provide power and control signals to and receive and record data from the hydrofoil's components. Connected to the servo rails are the speed pressure sensor (SPS) and depth pressure sensor (DPS), which are used to control the speed and height of the hydrofoil during flight. The servo rails also connect to the elevons (SERV), which are used to steer the hydrofoil during flight. The servo rails power the camera (CAM) and transmitter (CAM T) that allow the hydrofoil to record and transmit live footage. Lastly, the servo rails connect to the ESC and RMC to send control signals to the propeller motor and retraction mechanism motor.

B. Autopilot Hardware/Software

As described in the previous section, the Unmanned Foil is equipped with an electronic hardware package that allows it to be controlled remotely and, to some extent, autonomously. The two pressure sensors, installed in the fuselage of the vessel, measure depth and water-speed, which is critical to the subsequently discussed height control loop. The pilot can send commands to the vessel via a telemetry connection or through a long-range RC transmitter, which permits high latency manual control of the vessel. The telemetry modem is connected to a mission computer that runs a program called *Mission Planner*, which is used to plan autonomous missions and modify parameters in the autopilot software.

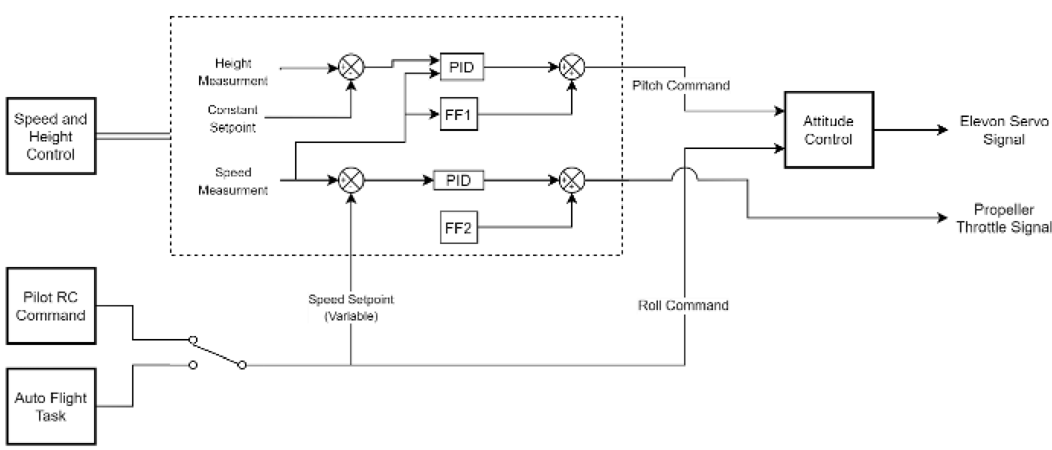

Figure 25. High-level block diagram detailing the integration of the Unmanned Foil's speed and height controller with pre-existing autopilot modules. PID denotes a proportional integral derivative controller while the blocks labeled FF indicate feedforward terms. FF1 utilized a theoretically derived relationship relating speed to trim pitch angle that

The software running on the Pixhawk autopilot is a customized version of the open source ArduPlane library [13]. ArduPlane, a subclass of the larger ArduPilot repository, is a versatile software package that is intended for the control of small to mid-scale fixed-wing drones. The package has a diverse library of sensor drivers, safety and logging features, and features that allow drones to be flown remotely. Towards the latter end, a hierarchy of flight modes let the pilot interact with the vessel with increasing degrees of autonomy. These modes include *Manual*, where no autopilot assistance is provided; *Fly By Wire A* (FBWA), which stabilizes the roll axis while the pilot controls pitch and throttle; and *Auto* mode, which is a completely hands off mode where the vessel conducts a mission that has been pre-programmed using Mission Planner.

While the stock ArduPlane software was, in many ways, applicable for the hydrofoil project, it was necessary to rework some key features. The primary alteration was the development of a speed and height control loop that uses measurements from the onboard pressure sensors as feedback. This new controller replaces the total energy speed and height control (TECS) system. Operational requirements of the hydrofoil necessitate that the vessel can travel for long periods of time at a constant velocity and a fixed height. The TECS is based on a typical fixed-wing control strategy, which is to change the pitch of the aircraft to gain speed. Initial testing showed that the TECS was ineffective for precision height holding with the hydrofoil, and thus the new controller was designed to decouple pitch and speed in the control loop.

Figure 25 gives a high-level overview of the new speed and height controller. The height controller regulates the depth of the fuselage, related to the height of the hull through the fully extended mast length, to a user-defined setpoint by commanding a pitch angle. Gain scaling and a feedforward trim term are used to improve performance and account for the velocity-dependent lift force. A low-level control loop converts the pitch demand to a signal for the elevons of the vessel. Meanwhile, the speed controller drives the measured water-speed to a setpoint defined by the position of a joystick on the RC transmitter. The speed controller used an experimentally derived feedforward term that was obtained by fitting a curve to steady-state water-speed data gathered at various fixed throttle settings.

IX. TESTING

Testing of the Unmanned Foil was conducted at Lake Wauburg in Gainesville, Florida, under permission from the University of Florida. Numerous cycles of testing were conducted to iteratively improve the hydrofoil control software and evaluate the robustness of the mechanical design. Trials were conducted at high speeds using the smaller set of wings, while slow speed testing was done with the large set of wings.

Control gains for the speed, height, and attitude controllers were iteratively tuned in the field. Since crashes of the vessel into the water were benign, this process could be done safely. A typical flight, as shown in Figure 26, begins with the boat at rest with fully extended mast, from which the pilot lifts the boat out of the water manually in FBWA mode. Then the speed and height controller are activated, and the autopilot regulates the height of the hull to the setpoint while speed and roll angle are commanded by the pilot. For the experiment in Figure 26, the gains of the height holding controller were tuned to reduce steady state error. Consequently, aggressive control action led to large overshoot of the setpoint before the system settled to a steady state. The RMS height error for the steady state portion of the trial shown in Figure 26 was 1.61 cm.

Autonomous missions were also a significant part of testing. The *Loiter* mission command, in which the autopilot attempts to fly the vessel in a circle of predefined radius, was used to create a controlled environment for evaluating new features. When flying circles of sufficiently large radius, as in Figure 27, the

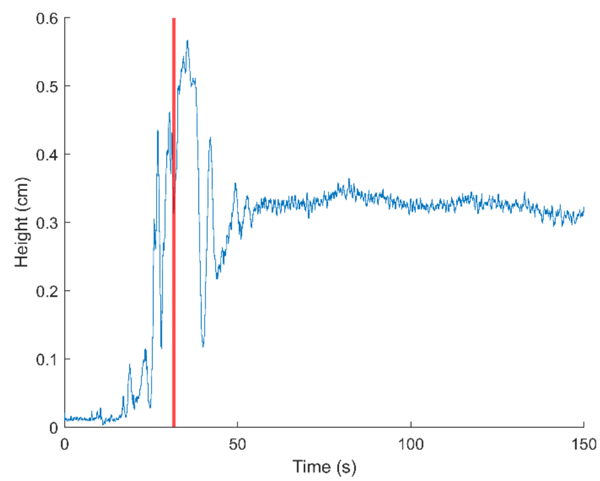

Figure 26. Representative flight segment. The vertical red line indicates the time when the speed and height controller was activated. A 1 sec. moving average filter has been applied to the data.

vessel's performance simulated straight-line flight. Waypoint tracking missions were conducted to evaluate the hydrofoil's ability to autonomously conduct turns of variable radius. Although this sequence of testing showed that the hydrofoil could conduct tight turns on the order of 5 meters in radius, a control strategy has not been developed that can achieve this performance consistently.

GPS speed, battery voltage and current data for testing similar to that of the *Loiter* mission in Figure 27 are shown in Figure 28. For a starting voltage of 45 V and a timed run of just over 3 min (200 s), the average vessel current draw was 20.7 A for an average cruising speed of 5.1 m/s (11.4 mph), and average battery power of 932 W. This current value is significantly less than the predicted value of 41.9 A, at 10 mph (Table VII). Differences are likely due to the OTS prop (and not the custom prop) being used for this test, a difference in the wing planform used for the final and initial vessels, and conservative assumptions made in simulating the prop torque. Comparing the graphs in Figure 28, we see that the methodology used for the drag-buildup and the propeller design were accurate. However, most runs were flown with the large wing and the OTS propeller. The decision to move to the large wing and OTS propeller was largely driven by control considerations. The smaller wing made the vessel difficult to control, and the custom propeller was designed for higher speeds. Hence, a larger wing and a lower speed propeller were needed to gain sufficient control. Despite these changes, the vessel still performed within design endurance goals. Were the test data obtained for the large wing and OTS propeller to be extrapolated across a 2-hour test, the 4, 46 A·h total on-board batteries would exceed design goals and achieve a test time of over 2.2 hours.

The requirements of the action components were previously highlighted in the design analysis and the experimental testing of the vessel demonstrates the

Figure 27. GPS data from an autonomous Loiter mission. The vessel was commanded to fly in a circle of 60m radius

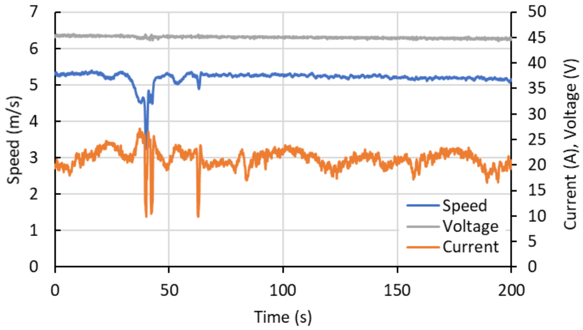

Figure 28. GPS and battery testing data for autonomous Loiter mission

robustness of this iteration. The telescoping mast mechanism consistently performed its duties through an appropriate range and rate while supporting dynamic loads. The mechanism offered a significant advantage during testing since the vessel could be launched in shallow water. By mapping the retraction motor and the reverse feature of the propeller ESC to switches on the RC transmitter, the vessel could be maneuvered to deeper water, where the mast was then fully extended.

One consequence of the externally mounted rack determined during testing is an unsymmetrical drag profile across the mast during flight. This characteristic was evident as the craft leaned to one side during steady flight and sprays water up from the rack. To counter this lean, a manually adjustable trim tab was bolted to the mast.

Despite significant efforts in the design phase and assembly submersion in a water trough, water intrusion was a prevalent issue during flight. Testing revealed that the hull compartments and mast hose were not as robust against heavy splashing as desired. However, procedures were developed to mitigate these issues. The elevon shaft sealing design proved ineffective. While the exact cause of this failure is unknown, it is notable that the clearance between shaft and housing was approximately 0.001 inches. This is significantly less clearance than recommended for O-rings in a dynamic rotary configuration [12]. The propeller shaft dynamic seal design never demonstrated an observable leak.

The most effective leak testing method devised consisted of covering suspected areas in soapy water and blowing compressed air through a port in the otherwise sealed fuselage. While this technique was enlightening, it did not simulate the performance of seals in dynamic conditions. As an observable dynamic testing configuration was difficult, conclusive data on the causes of water intrusion was not obtained. Remarkably, the hydrofoil withstood many flight tests despite significant water intrusion in the fuselage and occasionally in the hull.

X. FUTURE WORK

As discussed in Section III, the unique aspects of the hydrofoil provide the potential to be impactful in various applications. A future iteration is necessary to fulfill the potential of the Unmanned Foil and develop on the lessons learned. In this section we discuss design improvements inspired by the testing process.

In terms of autopilot software, some important features remain to be developed before the hydrofoil is feasible as an autonomous platform. First an autonomous takeoff mode needs to be implemented and integrated with Mission Planner as a mission command. Second, it is necessary to develop a raster path planning strategy to produce turns that the hydrofoil can repeatably conduct.

To better optimize the powertrain subsystem, the actual slip of both the OTS and custom propeller can be determined experimentally. If the vessel performs a timed run across a set distance of a mile, while maintaining a constant motor rpm, the fluid sliding losses with the propeller can be found, specific for this vessel's propeller. From this value, the propeller pitch and propeller rpm can be better estimated for our vessel. With a more appropriate propeller, the efficiency of this system will increase, and the endurance time of vessel can be improved upon further.

Following analysis of the flight test results, the design of the control surfaces and retraction mechanism can be improved. In the case of the elevons, extreme banking during flight leads to breaking the water surface with the elevon tips resulting in reduced control effectiveness. A lower mounting of the tail, or adding some anhedral angle, despite potential issues with roll stability, could offer a potential net gain in controllability by alleviating water breaking issues. The retraction mechanism contributed to asymmetrical drag due to the rack. Improvements to this design can be achieved with rollers along the quarter chord of the mast airfoil. However, it is important that the roller design has accurate positioning and minimal slippage of the mast. As a proof of concept, testing of a roller design was conducted with hardness of the rubber rollers and clamping force acting normal to the mast as variables.

To prevent leaking, the elevon seals would be redesigned to include true dynamic seals. Additionally, there would be increased clearance in the elevon housing, creating a grease chamber that can trap water. Although there were less issues with the propeller dynamic seal, a redesign would use back to back dynamic seals to create a more effective grease chamber configuration. Grease ports could be added to allow for pumping of fresh grease into the chamber without requiring disassembly.

XI. CONCLUSION

This paper has described the design and testing of an autonomous hydrofoil by a student team at the University of Florida. The design of this system required knowledge from a range of fields including aerodynamics, mechanical design, composite manufacturing, power systems, software development, and control design. The vessel has targeted applications for surveys and mapping.

The hydrofoil concept shows great potential. At the time of writing, the current hydrofoil prototype has reached end-of-life due to failures induced by a heavy testing cycle. Primarily, water intrusion proved to be an issue that could not be eliminated in the current prototype. Given the opportunity to iterate on the design, the team believes these issues can be resolved.

XII. ACKNOWLEDGEMENTS

We would like to thank our faculty advisor, Dr. Peter Ifju, for his inspiration for this project and dedication in seeing its completion. Without his help, this project would not have been possible.

Axton Isaly received the B.S. in Mechanical Engineering from the University of Florida in 2019. As the controls lead, he programmed the autopilot and conducted flight tests.

Sebastian Deleon received the B.S. in Mechanical Engineering from the University of Florida in 2019. As the electronics lead, he designed and assembled the electronic hardware package.

Antonio Diaz received the M.S. in Aerospace Engineering from the University of Florida in 2017. As the actuation mechanisms lead, he was responsible for the elevon and mast retraction mechanisms.

Moses Divaker is pursuing the Ph.D. in Aerospace Engineering from the University of Florida. As the hydrodynamics lead, he performed critical dynamic modeling.

Ryan Earl received the B.S. in Mechanical Engineering from the University of Florida in 2018. As the powertrain lead, he helped design the battery-motor-gearbox subassembly, as well as the custom propeller.

Lucas Murphy received the B.S. in Mechanical Engineering from the University of Florida in 2018. As the hull lead, he designed and built all aspects of the hull.

Andrew Ortega will receive the B.S. in Computer Science from the University of Florida in 2020. As the remote sensing lead, he researched and tested potential sensor packages for bathymetric mapping.

XIII. REFERENCES

[1] "Lift eFoil," Lift, [Online]. Available: https://liftfoils.com/efoil/. [Accessed 15 June 2020].

[2] R. Hunter, C. Brown, L. Jenkins, G. Meadows and R. Shuchman, "BathyBoat: An Autonomous Surface Vessel for Stand-alone Survey and Underwater Vehicle Network Supervision," *Marine Technology Society Journal*, vol. 44, pp. 20-29, 2010.

[3] J. Melo and A. Matos, "Guidance and control of an ASV in AUV tracking operations," in *OCEANS*, 2008.

[4] M. Johnson-Roberson, O. Pizarro, S. B. William and I. Mahon, "Generation and visualization of large-scale three-dimensional reconstructions from underwater robotic surveys," *Journal of Field Robotics*, vol. 27, pp. 21-51, 2010.

[5] J. D. Anderson, Fundamentals of Aerodynamics, New York: McGraw-Hill, 1991.

[6] S. F. Hoerner, Fluid-Dynamic Drag, Brick Town: Hoerner Fluid Dynamics, 1965.

[7] S. Gudmundsson, General Aviation Aircraft Design: Applied Methods and Procedures, Butterworth-Heinemann, 2013.

[8] OpenVSP Team, "OpenVSP Main Page," [Online]. Available: http://openvsp.org/. [Accessed 28 June 2020].

[9] D. Gerr, "Propellor Handbook: The Complete Reference for Choosing, Installing, and Understanding Boat Propellors.," *International Marine*, 1989.

[10] B. P. Epps and R. W. Kimball, "OpenProp v3: Open-source software for the design and analysis of marine propellers and horizontal-axis turbines," (2013). [Online]. Available: http://engineering.dartmouth.edu/epps/openprop.

[11] E. T. Tupper, Introduction to Naval Architecture, Fifth Edition, Butterworth-Heinemann, 2013.

[12] Parker Hannifin Corporation, "Parker O-Ring Handbook," Lexington.

[13] Ardupilot, "Plane Home," [Online]. Available: ardupilot.org/plane. [Accessed 15 May 2020].

XIV. APPENDIX

Figure A1. Labelled view of Unmanned Foil components.